Buried graphene electrode heater for a polymer waveguide thermo-optic device

WANG, Xibin; JIN, Wei; CHANG, Zeshan; CHIANG, Kin Seng

Published in:
Optics Letters

Published: 15/03/2019

Document Version:
Post-print, also known as Accepted Author Manuscript, Peer-reviewed or Author Final version

Published version (DOI):
10.1364/OL.44.001480

Publication details:
WANG, X., JIN, W., CHANG, Z., & CHIANG, K. S. (2019). Buried graphene electrode heater for a polymer waveguide thermo-optic device. *Optics Letters*, *44*(6), 1480-1483. Advance online publication. https://doi.org/10.1364/OL.44.001480

Buried graphene electrode heater for polymer-waveguide thermo-optic device

XIBIN WANG, WEI JIN, ZESHAN CHANG, AND KIN SENG CHIANG*

Department of Electronic Engineering, City University of Hong Kong, 83 Tat Chee Avenue, Hong Kong SAR, China
** Corresponding author: eeksc@cityu.edu.hk*

Received XX Month XXXX; revised XX Month, XXXX; accepted XX Month XXXX; posted XX Month XXXX (Doc. ID XXXXX); published XX Month XXXX

We propose the use of graphene as the electrode heater material for a polymer-waveguide thermo-optic (TO) device. Because a graphene electrode can be buried in a polymer waveguide without introducing a significant loss to the transverse-magnetic polarized light, we can do away with the buffer layer that is required in a conventional TO device to isolate the metal electrode heater from the waveguide and, hence, reduce the driving electric power of the device. To demonstrate the principle, we fabricate and compare two polymer-waveguide TO mode switches based on the configuration of a balanced Mach-Zehnder interferometer, which are identical except that one uses a buried graphene electrode and the other uses an aluminum electrode deposited on the waveguide surface. Our experimental device that uses a graphene electrode has a switching power almost four times lower and also responds faster. The use of buried graphene electrodes is an effective approach to reducing the power consumption of TO devices.

OCIS codes: (130.3120) Integrated optics devices; (130.5460) Polymer waveguides; (130.4815) Optical switching devices; (160.6840) Thermo-optic materials.

Optical polymers are attractive materials for the realization of integrated optics devices, thanks to their many advantages, such as simple fabrication process, low cost, low optical loss, and small birefringence [1]. Their large thermo-optic (TO) coefficient and low thermal conductivity, in particular, allow the construction of efficient thermally tunable devices [2]. Polymer-waveguide TO devices have found numerous applications as optical switches and variable optical attenuators in optical signal processing and optical communication systems [3,4]. The electrode heater used in a conventional polymer TO device is made of metal. To minimize the applied electric power for heating, the electrode should be placed as close to the waveguide core as possible. To avoid excess metal-induced light-absorption, a sufficiently thick polymer buffer layer must be placed between the waveguide core and the electrode, which, however, limits the heating efficiency. In this letter, we propose the use of graphene as the electrode heater material for the realization of a polymer-waveguide TO device. The graphene electrode can be buried in a polymer waveguide without inducing a significant optical loss, which can thus improve the heating efficiency of the device. By doing away with the buffer layer, we can truly minimize the driving electric power of the device.

Our proposed idea is based on the recent finding that graphene strongly attenuates the propagating wave whose major electric field is parallel to its surface, namely the transverse-electric (TE) waves, while introduces little loss to the propagating wave whose major electric field is perpendicular to its surface, namely the transverse-magnetic (TM) waves [5]. As a single layer of carbon atoms, graphene does not allow any electric current flowing in the normal direction and, therefore, does not dissipate the normal electric-field component of the propagating wave. Such a property of graphene has been applied to the realization of ultra-broadband mode filters [6] and lithium-niobate electro-optic devices [7]. Graphene's excellent thermal and electrical conductivity and mechanical stability have also been exploited for forming graphene electrode heaters in silicon photonic devices [8–14], but the large index contrast of silicon waveguides does not allow the existence of pure TM and TE waves and the graphene-induced losses in such devices are significant. On the other hand, the low index contrast of polymer waveguides allows negligible graphene-induced loss to the TM waves, even though graphene is buried in the waveguide core [5,6]. To demonstrate our idea, we designed and fabricated two polymer-waveguide TO mode switches based on the configuration of a Mach-Zehnder interferometer (MZI) with one using a buried graphene electrode and the other using an aluminum (Al) electrode deposited on the waveguide surface. Our experiments show that the use of a graphene electrode lowers the switching power of the device by almost four times and also shortens the response time of the device.

Figure 1 is a schematic diagram of the TO mode switch, which is a balanced MZI constructed with two identical symmetric waveguide Y-junctions connected back-to-back. Each Y-junction is formed with a two-mode core of width w_1 at one end, which branches out into two identical single-mode cores of width w_2 with S-bends and at the other end. Two identical electrode heaters are

deposited on the two straight arms of the MZI to ensure the balance of the MZI, though only one heater is actually needed for the operation of the switch. The two electrode heaters have the same width of 15 μm and the same length of 4 mm. The device is designed for the TM polarization. The two-mode waveguides in the device support the TM_{11} and TM_{21} modes, while the single-mode waveguides support only the TM_{11} mode. When either the TM_{11} or the TM_{21} mode is launched into the two-mode waveguide at the input end, it is split into two identical halves by the Y-junction, which then propagate as the TM_{11} modes along the two single-mode waveguide arms, respectively. By applying electric power to the heater along one arm, we can change the refractive-index difference between the two arms through the TO effect and hence the phase difference between the TM_{11} modes of the two arms. Without applying electric power to the heater (the OFF state), the phase difference between the two arms is 0 for the TM_{11} mode input or π for the TM_{21} mode input, which means that the output mode from the MZI is the same as the input mode. When a suitable electric power is applied to the heater to induce a π-phase change between the two arms (the ON state), the output mode is switched from the launched mode into the other mode. The device thus functions as a mode switch between the TM_{11} and TM_{21} modes. The function of the device is summarized in Table 1.

Figure 2(a) shows the cross section of an MZI arm for a conventional design that uses an Al electrode heater. The core and cladding refractive indices are chosen to be 1.569 and 1.559, respectively, which are the refractive indices of the polymer materials used in the experiments. The lower cladding is fixed at

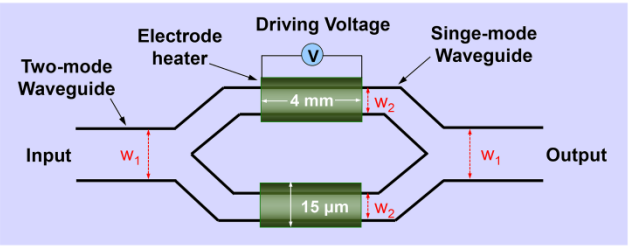

Fig. 1. Schematic diagram of the polymer-waveguide TO mode switch, which is a balanced MZI formed with two Y-junctions connected back-to-back.

Table 1. Function of the mode switch

Input mode		Switch state	Output mode	
TM_{11}		ON	TM_{21}	
		OFF	TM_{11}	
TM_{21}		ON	TM_{11}	
		OFF	TM_{21}	

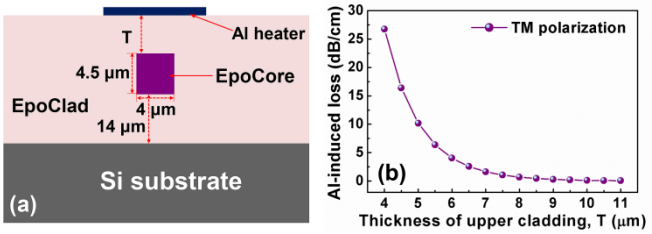

Fig. 2. (a) Cross section of an MZI arm for a conventional design, where an Al electrode heater is placed on the surface of a thick upper cladding; (b) variation of the Al-induced loss to the TM_{11} mode with the thickness of the upper cladding T, calculated at 1550 nm.

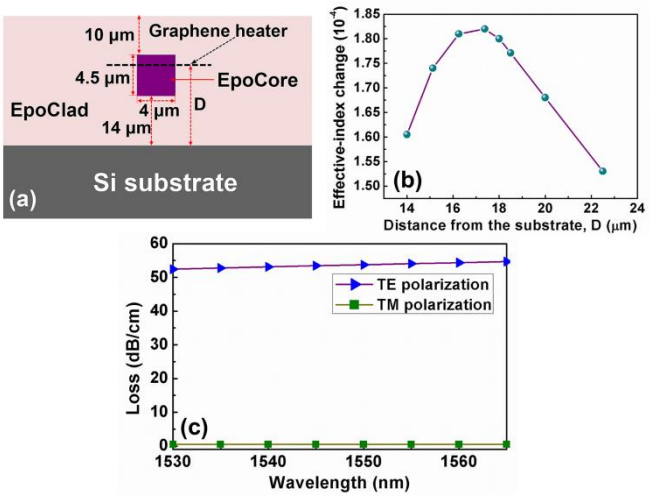

Fig. 3. (a) Cross section of an MZI arm for the proposed design, where a graphene electrode heater is buried in the waveguide; (b) variation of the change in the effective index of the TM_{11} mode with the distance of the graphene heater from the substrate D, calculated at an applied electric power of 2 mW; (c) losses of the TM_{11} and TE_{11} modes in the C-band induced by a 4-mm-long graphene electrode, calculated for the graphene location D = 18.5 μm.

14 μm to avoid excess mode leakage to the high-index silicon substrate. The single-mode cores of the MZI have a width of w_2 = 4.0 μm and the two-mode cores at the two ends of the MZI have a width of w_1 = 8.0 μm. All the cores have the same thickness of 4.5 μm. As shown in Fig. 2(a), an upper cladding is placed between the core and the Al electrode to reduce the Al-induced loss to the guided mode. Figure 2(b) shows the calculated Al-induced loss to the TM_{11} mode as a function of the thickness of the upper cladding with the commercial software COMSOL, where the refractive index of Al is set at 1.44 + 16i (for 1550 nm). To keep the Al-induced loss lower than 0.1 dB/cm, the thickness of the upper cladding should be larger than ~10 μm. This thick upper cladding of polymer inevitably reduces the efficiency of the heater and thus increases the driving electric power.

We next consider the design that uses a buried graphene electrode heater. Figure 3(a) shows the cross section of an MZI

arm for the proposed design. The waveguide materials and dimensions are identical to those for the conventional design. To study how the location of the graphene electrode affects the heating efficiency, we fix the driving electric power at 2 mW and calculate the temperature distribution in the waveguide for a given graphene location using the heat transfer module in COMSOL, where the thermal conductivities of the polymer waveguide and the silicon substrate are set at 0.12 W/(m·K) and 163 W/(m·K), respectively. With the knowledge of the temperature distribution, we calculate the thermally induced change in the effective index of the TM_{11} mode with the mode solver in COMSOL, where the TO coefficient of the polymer waveguide is set at 1×10^{-4}/°C. The variation of the thermally induced change in the effective index of the TM_{11} mode with the distance of the graphene electrode from the substrate D, calculated at 1550 nm, is shown in Fig. 3(b). The change in the effective index is proportional to the phase change of the TM_{11} mode propagating along the MZI arm and, therefore, is a measure of the heating efficiency. As shown in Fig. 3(b), the maximum change in the effective index occurs at D = 17.4 μm, which is closed to the top surface of the core. In practice, it is much easier to place a graphene electrode on top of the core (D = 18.5 μm) than embed it in the core. In our fabrication work, we choose D = 18.5 μm with a slight sacrifice of the heating efficiency. We also calculate the graphene-induced optical losses with the mode solver in COMSOL, where the graphene electrode is modeled as a conductive boundary with a complex surface conductivity of $6.084 \times 10^{-5} - 7.519 \times 10^{-6}i$ at 1550 nm [5,7]. Figure 3(c) shows the losses of the TM_{11} and TE_{11} modes over the C-band induced by a 4-mm-long graphene electrode placed on the top surface of the core. The graphene-induced loss to the TE_{11} mode is larger than 50 dB/cm, while that to the TM_{11} mode is smaller than 1 dB/cm. As expected, the graphene electrode heater does not cause a significant loss to the TM mode. Our proposed device operates for the TM polarization while blocking the TE polarization.

We followed the design parameters and fabricated the devices with the polymer materials EpoCore and EpoClad (Micro Resist Technology) as the core and the cladding material, respectively, using the standard microfabrication processes. EpoClad was first spin-coated onto an O_2-plasma treated silicon substrate and cured to from a 14-μm-thick lower cladding. EpoCore was next spin-coated onto the lower cladding and cured to form a 4.5-μm-thick core layer. The EpoCore layer was etched into waveguide cores with the desired widths by the standard photolithography and wet-etching processes. EpoClad was then spin-coated onto the sample and cured to form a 10-μm-thick upper cladding. To fabricate the device that employs an Al electrode, an Al film with a thickness of ~100 nm was deposited onto the upper cladding by thermal evaporation and patterned into two separate Al electrodes along the respective arms of the MZI by photolithography and wet-etching. Each Al electrode had a width of 15 μm and a length of 4 mm. For the device that employs a graphene electrode, the upper cladding was first etched to expose the core by reactive ion etching (RIE). The exposed core and side-cladding area was then covered with graphene. The mono-atom graphene film used (Hefei Vigon Tech.) in our experiment had a size of 10 mm × 10 mm and came as an attachment to a polymethylmethacrylate (PMMA) buffer. To transfer the graphene film onto the waveguide sample, the buffer was floated in deionized water and fished by the sample [5]. The PMMA buffer was then dried and removed from the sample with acetone. Cu contacts were deposited onto the graphene film by metal deposition and the graphene film was patterned into two separate electrodes (each with a width of 15 μm and a length of 4 mm) along the respective arms of the MZI by photolithography and RIE. Finally, EpoClad was spin-coated onto the graphene-covered sample to resume the 10-μm-thick upper cladding and the Cu contacts were exposed for probing by removing the upper cladding above the contacts by photolithography and wet etching. The device had a total length of 21 mm, which included a 5-mm-long two-mode waveguide lead at each end of the MZI. Reference waveguides of the same dimensions without any electrodes were also fabricated for comparative studies. Figure 4(a) and 4(b) show the cross sections of two fabricated waveguides, which incorporate, respectively, an Al electrode and a graphene electrode.

To characterize the performances of the fabricated devices, the output light from a tunable semiconductor laser (KEYSIGHT) was launched into the device under test to excite only the TM_{11} mode with a lensed single-mode fiber (SMF). Polarization optics was used to ensure that the light launched into the waveguide was TM-polarized. The output light from the device was focused onto an infrared camera with a lens to obtain near-field patterns or coupled to an optical power meter with an SMF for optical power measurement. By comparing the output powers of a graphene-embedded waveguide and a reference waveguide, we found that the graphene-induced loss to the TM_{11} mode over the C-band was smaller than 1 dB and that to the TE_{11} mode was larger than 25 dB, in good agreement with the calculation results.

To demonstrate the mode-conversion function of the devices, we launched the laser light into the device under test to excite only the TM_{11} mode and drove the device at different electric powers. Figures 5(a) and 5(b) show the output near-field images taken at

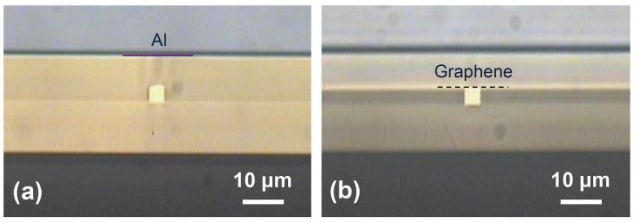

Fig. 4. Cross sections of two fabricated waveguides, which incorporate, respectively, (a) an Al electrode and (b) a graphene electrode.

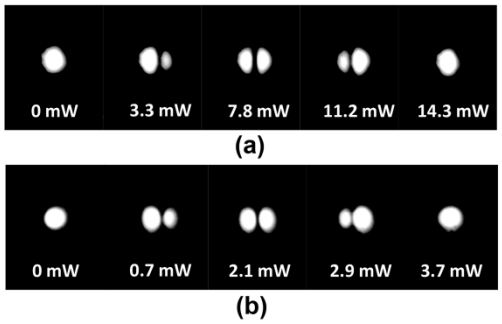

Fig. 5. Output near-field images taken at different driving electric powers at 1550 nm for the devices that use (a) an Al electrode and (b) a graphene electrode.

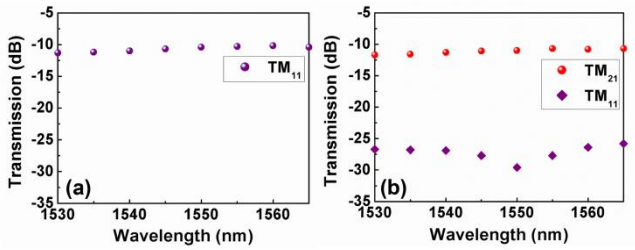

Fig. 6. Normalized transmission spectra of the device that uses a graphene electrode, measured at the (a) OFF and (b) ON states with the TM_{11} mode as the input mode.

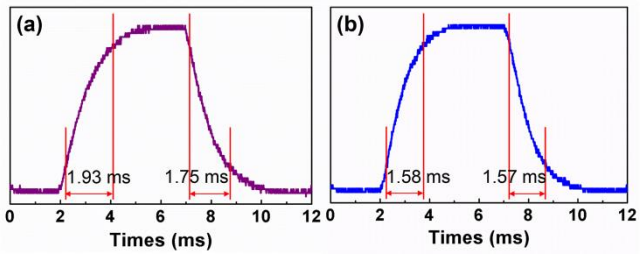

Fig. 7. Temporal switching characteristics of the mode switches that use (a) an Al electrode and (b) a graphene electrode.

1550 nm for the devices that use an Al electrode and a graphene electrode, respectively. The results in Fig. 5 confirm that both devices operate as a TM_{11}-TM_{21} mode switch. For the switch that uses an Al electrode, the switching power required is ~7.8 mW, while for the device that uses a graphene electrode, the switching power is ~2.1 mW. The use of a graphene electrode reduces the switching power by almost four times. We also measured the output powers of the device that uses a graphene electrode at different wavelengths. Figures 6(a) and 6(b) show the measured output powers normalized to the TM_{11} input power for the OFF and ON states of the switch, respectively. At the OFF state, the TM_{11} mode does not convert into the TM_{21} mode and has an insertion loss of 10.4 dB (which includes fiber-waveguide coupling losses at both ends) at 1550 nm, as shown in Fig. 6(a). At the ON state, the TM_{11} mode is converted into the TM_{21} mode with a conversion efficiency of 98.7% and an insertion loss of 10.8 dB at 1550 nm. Over the C-band, the mode extinction ratio is higher than 15.2 dB and, at 1550 nm, the mode extinction ratio reaches 18.6 dB. The actual mode extinction ratio should be higher, considering the difficulty of achieving 100% mode purity in launching the TM_{11} mode into the two-mode waveguide of the device. The insertion loss of the device is mainly due to the roughness along the waveguide introduced in the fabrication process and the relatively large absorption loss of the polymer materials in the C-band (1 – 2 dB/cm). It should be possible to reduce the loss of the device by improving the fabrication process and using low-loss polymer materials developed for the C-band [15].

We finally measured the response times of the devices by applying a square-wave switching signal at 100 Hz to the electrode heater and monitoring the output signal with a photodetector and an oscilloscope. The temporal switching characteristics of the devices that use an Al electrode and a graphene electrode, displayed by the oscilloscope, are shown in Fig. 7(a) and 7(b), respectively. As shown in Fig. 7(a), the rise and fall times of the switch that uses an Al electrode are 1.93 and 1.75 ms, respectively, while the rise and fall times of the switch that uses a graphene electrode are 1.58 and 1.57 ms, respectively. The lower switching power obtained from using a graphene electrode also helps to reduce the response time. It should be possible to reduce the response time of the device by an order of magnitude by employing a hybrid strip-waveguide structure [16].

In conclusion, we have proposed the use of graphene electrode heaters for the realization of polymer-waveguide TO devices. A graphene electrode can be buried in a polymer waveguide to significantly increase the heating efficiency without inducing a significant loss to the TM modes, which cannot be achieved with a conventional metal electrode or transparent electrode (e.g., an indium-tin-oxide electrode). We have demonstrated the idea with a TO mode switch based on the configuration of a balanced MZI. Our fabricated devices show that the switching power obtained with a graphene electrode is almost four times lower than that obtained with an Al electrode and the response of the device that uses a graphene electrode is also faster. The use of buried graphene electrodes is an effective approach to forming efficient TO devices based on polymer or low-index contrast material systems.

Funding. Research Grants Council, University Grants Committee (RGC, UGC), Hong Kong (CityU 11202014, CityU 11205715). Xibin Wang is on leave from Jilin University, China, under the Hong Kong Scholars Program (No. XJ2016026).

References

1. H. Ma, A. K.-Y. Jen, and L. R. Dalton, Adv. Mater. **14**, 1339 (2002).
2. Z. Zhang and N. Keil, Opt. Commun. **362**, 101 (2016).
3. X. Wang, J. Sun, Y. Liu, J. Sun, C. Chen, X. Sun, F. Wang, and D. Zhang, Opt. Express **22**, 11119 (2014).
4. D. Li, Y. Zhang, L. Liu, and L. Xu, Opt. Express **14**, 6029 (2006).
5. Z. Chang and K. S. Chiang, Opt. Lett. **41**, 2129 (2016).
6. Z. Chang and K. S. Chiang, Opt. Lett. **42**, 3868 (2017).
7. Z. Chang, W. Jin, and K. S. Chiang, Opt. Lett. 43, 1718 (2018).
8. Q. Yang, L. Qin, G. Cao, C. Zhang, and X. Li, Opt. Lett. **43**, 639 (2018).
9. Z. Xu, C. Qiu, Y. Yang, Q. Zhu, X. Jiang, Y. Zhang, W. Gao, and Y. Su, Opt. Express **25**, 19479 (2017).
10. L. Yu, D. Dai, and S. He, Appl. Phys. Lett. **105**, 251104 (2014).
11. S. Yan, X. Zhu, L.H. Frandsen, S. Xiao, N. A. Mortensen, J. Dong, and Y. Ding, Nat. Commun. **8**, 14411 (2017).
12. L. Yu, Y. Yin, Y. Shi, D. Dai, and S. He, Optica **3**, 159 (2016).
13. L. Yu, J. Zheng, Y. Xu, D. Dai, and S. He, ACS Nano **8**, 11386 (2014).
14. H. Li, Y. Anugrah, S.J. Koester, and M. Li, Appl. Phys. Lett. **101**, 111110 (2012).
15. D. de Felipe, M. Kleinert, C. Zawadzki, A. Polatynski, G. Irmscher, W. Brinker, M. Moehrle, H. G. Bach, N. Keil, and M. Schell, J. Lightw. Technol. **35**, 683 (2017).
16. Q. Xu, M. Jiang, D. Niu, X. Wang, L. Wang, K. S. Chiang, and D. Zhang, Opt. Lett. **43**, 5102 (2018).